

Geometrical analysis of sand piles on small platforms

John M. H. Barton and Steven G. Buchberger

Department of Civil and Environmental Engineering, University of Cincinnati, P.O. Box 210071, Cincinnati, Ohio 45221-0071, USA

(Received 7 March 2003; published 18 July 2003)

The underwater geometry of small sand piles is relevant to the removal of noncolloidal sediment by filtration. The critical size range for clogging occurs when noncolloidal particles are about one-tenth the diameter of the media grains. No previous experimental work has examined the formation of sand piles at this scale. Sand pile formation was investigated on small platforms (roughened spheres, flat surfaces, and irregular stones) in the critical size range for clogging. The size of sand piles formed on platforms of irregular crushed stone increases with sand grain diameter. This did not occur for spherical media. Further, this observation contrasts with previous measurements of the angle of repose, which showed a weak decrease with sand grain size. A geometric model for small piles is presented to account for the increase in size of the sand pile as a function of grain size and platform shape.

DOI: 10.1103/PhysRevE.68.011303

PACS number(s): 45.70.Ht, 45.70.Cc

I. INTRODUCTION

This paper investigates the behavior of small piles of sand on various underwater platforms, focusing on the stability of the toe of slope. The behavior of these small piles is fundamental to the clogging and performance of filter media (e.g., gravel in french drains and infiltration trenches) by noncolloidal sediment (sand). The mechanisms which influence the formation of small piles help to explain the improved filter performance of crushed materials. During filtration, small piles accumulate on the leading edge of individual media grains and slough in avalanches, potentially clogging pore openings of the filter. If the sand grains are too small, these avalanches pass through without clogging. On the other hand, if the sand grains are too large, they are trapped at the filter surface and cause complete clogging. The critical size between passing through and complete clogging occurs where the average radius of the sand grains r_s is about one-tenth the average radius of the media grains r_m [1–3]. Near this critical size, several sand grains are necessary to bridge across a pore opening.

There has been no experimental work to study the geometry of sand piles at the scale of the critical size range for clogging. This work presents a geometric small pile model, which accounts for observations made at this critical scale. In particular, the aim of this paper is to demonstrate, both theoretically and experimentally, that the sand pile size increases with r_s , in the critical size range. This effect occurs when the media grains provide a stable toe of slope. A stable toe of slope is achieved only with crushed media, not with spherical media. The small pile model is scalable for the shape of a sand pile. Further, it is the only model that can be scaled from a large pile to make accurate predictions for small piles as a function of grain size and platform shape. The small pile model provides improved predictions of pile size than the standard cone model for a sand pile.

II. PREVIOUS WORK

Grains added to a pile of sand increase the slope of the pile to the angle of movement i . At that threshold, the pile

does not shed each new sand grain individually; rather, the sand pile sloughs many grains in an avalanche reducing the slope to the angle of repose i_r . Several authors give descriptions of these angles [4,5]. Both angles are related to the internal friction of the sand grains [6]. In most instances i exceeds i_r by several degrees [4]. When sand grains are sufficiently large, a single grain can change the slope from i_r to i [5].

Difficulties which occur when measuring i include: indeterminate end point, pile instability, and asymmetric piles [7]; therefore, experiments typically measure i_r for the slope of the sand pile as shown in Figs. 1(a)–1(e). Measurements reveal that i_r decreases slightly as r_s increases [7–12], but this size effect is relatively weak and easily obscured by other factors [7]. Underwater, a slight increase in i has been

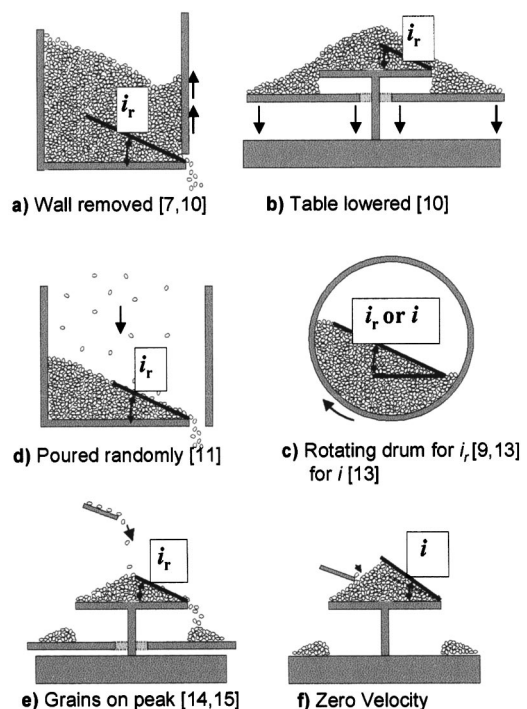


FIG. 1. Various experimental methods for sand piles.

TABLE I. Particles tested by various authors.

Source	Size range (S)	Notes
[1–3]	5–15	Critical size for clogging in filtration
This research	3.5–50	Sand
[5]	60 ^a	Theoretical calculation
[7]	50–160	Sand, shot, wood blocks
[8]	250–2000	Sand, shot, seed
[9]	33–17 000 ^b	Spheres, sand, cubes, powders
[10]	40–1000	Glass beads, DEM simulation
[11]	Very fine powders	Cohesive powders
[13]	20–2000 ^b	Spheres of glass and nylon
[14]	10–70	Aluminum oxide
[15]	25–40	Glass beads, shot

^aAt this value of S , the authors assume pile behavior changes from a small pile to a large pile.

^bDiameter of the drum used in calculation of S .

demonstrated with an increase in particle size [13]. Table I summarizes the size of sand grains and other particles used in the experiments by various authors. Figure 1 shows various experimental methods used to build a pile.

Differences have been observed in both the frequency and the mass of particle avalanches when piles are very small [14,15]. These differences have been attributed to a pile size effect [5]. However, they may simply be an artifact of the experimental method because the distance from the release point to the pile summit decreased as the pile size increased [14].

III. SAND PILE NOTATION

It is helpful to normalize r_m (the radius of the filter media grains or the platform on which the sand pile is formed) by r_s , the radius of the sand grains. This is reported as the specific size S shown in Eq. (1),

$$S = r_m / r_s. \quad (1)$$

Using this definition, the region of interest for this investigation (near the critical size) is $\approx 5 < S < 15$ [2]. As a definition $S < 60$ will be referred to as a small pile (sand grains on a small plate) and $S > 60$ as a large pile (sand grains on a large plate) [5].

For irregular media, r_m is given by

$$r_m = (A_m / \pi)^{1/2}, \quad (2)$$

where A_m is the presenting cross section of the irregular platform or media grain. Similarly, it is convenient to normalize the volume of the sand pile relative to the size of the platform. The specific depth D is defined as the average depth of the sand pile (see Fig. 2) in units of platform radii.

$$D = V / (A_m r_m), \quad (3)$$

where V is the total volume of the sand pile including space between the sand grains, given by

$$V = m / \rho(1 - \varepsilon). \quad (4)$$

Here, m is the mass of the sand pile, ρ is the density of the sand grains (specific gravity of the solids times the density of water), and ε is the effective porosity of the pile. Putting Eq. (4) into Eq. (3) gives D as a function of the mass of sand in a pile,

$$D = m / [\rho(1 - \varepsilon)A_m r_m]. \quad (5)$$

IV. PILE GEOMETRY ON A SMALL PLATFORM

The model of a sand pile on a filter media grain must consider three cases: the two extreme cases of a flat circular plate and of a sphere, and the more general case where the shape is irregular, something between a flat plate and a sphere. The following development considers first the case of the flat circular plate, then the case of the sphere, and finally combines them. Two models are presented for comparison: the cone model and the small pile model. Again the small pile model is so named, not because it applies only to small piles, but rather because it is scalable from large piles and still applies to small piles. Both models will be tested against actual measurements.

A. Specific depth D_p on a circular level platform

A simple geometric model of an inverted cone (base angle i) on a circular platform accurately represents the maximum size of a large sand pile. This cone is shown in Fig. 2. With the origin of the coordinate axes at the center of the platform, the height of the cone y_c at any point is given by

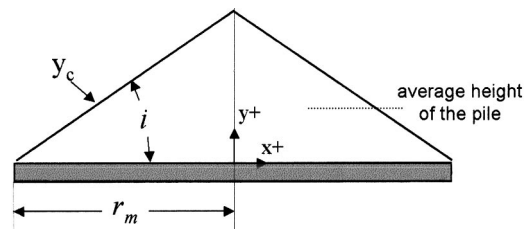


FIG. 2. A cone with origin at the center of the platform. D is the average height of the pile divided by platform radius r_m .

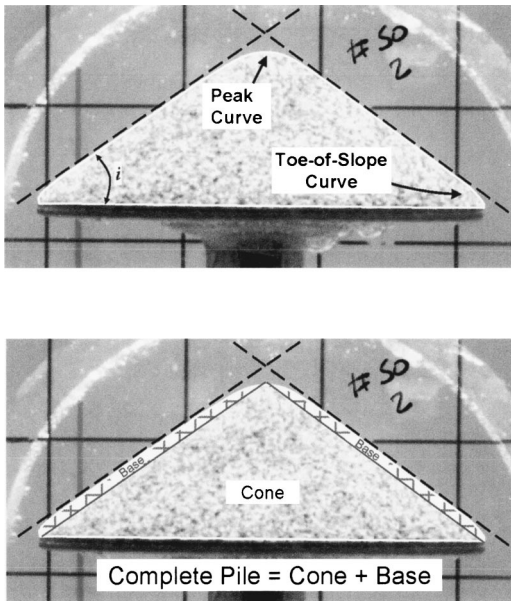


FIG. 3. Deviations from the cone model can be seen at the peak and at the toe of slope. The complete pile is the sum of the cone plus the base (hatched area). Although the base is drawn on top, it results from the toe of slope.

$$y_c = (r_m - |x|) \tan i. \tag{6}$$

The volume of this cone V_c as a surface of revolution is given by

$$V_c = 2\pi \int_0^{r_m} x y_c dx, \tag{7}$$

which gives

$$V_c = \frac{1}{3} \pi r_m^3 \tan i. \tag{8}$$

Using Eq. (3), this can be converted to a specific depth

$$D_c = \frac{1}{3} \tan i. \tag{9}$$

In the range of the experimental results provided later in the paper, i is shown to increase $\approx 2^\circ$ as r_s decreases [13]. Thus, a plot of D_c vs S will have a small slope.

Inspection of the actual shape of a sand pile (shown in Fig. 3) reveals deviation from a cone. The relatively linear surface of the cone separates small curves at the peak and the toe of slope.

When the pile is large, the effect of these curves on the total pile size is minimal and calculations based on a simple cone will be accurate approximations. However, as the size of the pile shrinks, these curves affect an increasing percentage of the pile profile. Eventually, these curves overlap and the linear side slope disappears. It is precisely in this region ($S \sim 10$), that an accurate model of the shape of the pile is needed.

The effect of the curves is to increase the mass of sand in the pile by raising the base of the cone up some distance as shown in Fig. 4. For large piles, the contribution to the total mass by the base (although small) can be approximated by a

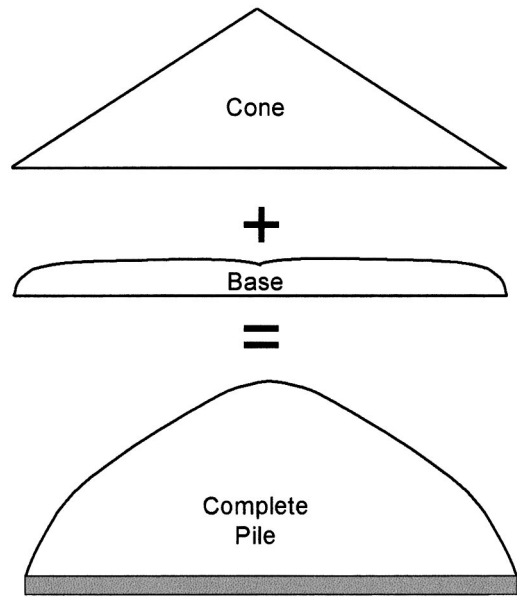


FIG. 4. Complete pile.

cylinder. However, for small piles the cylinder approximation will fall apart and an accurate description of the curvature is necessary. These curves can be closely approximated as hyperbolas [8].

First, consider the curve at the toe of slope. The shape of the curve at the toe of slope is shown in Fig. 5 as well as the contribution of the curve to the base with the cone removed. The hyperbola has two asymptotes. The first is horizontal at $y = a$ and the second vertical at $|x| = b + r_m$, that is, the vertical asymptote is shifted a distance b from the corner of the plate. Thus, the contribution of the toe-of-slope curve to the height of the base is given by

$$y_L = \frac{a(r_m - |x|)}{b + r_m - |x|}. \tag{10}$$

The shape of the toe of slope does not depend on the size of the particles as schematically represented in Fig. 6, thus the parameters a and b can be normalized by r_s .

$$\bar{a} = \frac{a}{r_s}, \tag{11}$$

$$\bar{b} = \frac{b}{r_s}. \tag{12}$$

These dimensionless coefficients will be used in what follows.

Second, the shape of the base must be corrected for the curve at the peak of the pile. The peak is shown in Fig. 7. The equation for the peak hyperbola with the cone removed is given as

$$y_u = |x| \tan i - \sqrt{c^2 + x^2 \tan^2 i}. \tag{13}$$

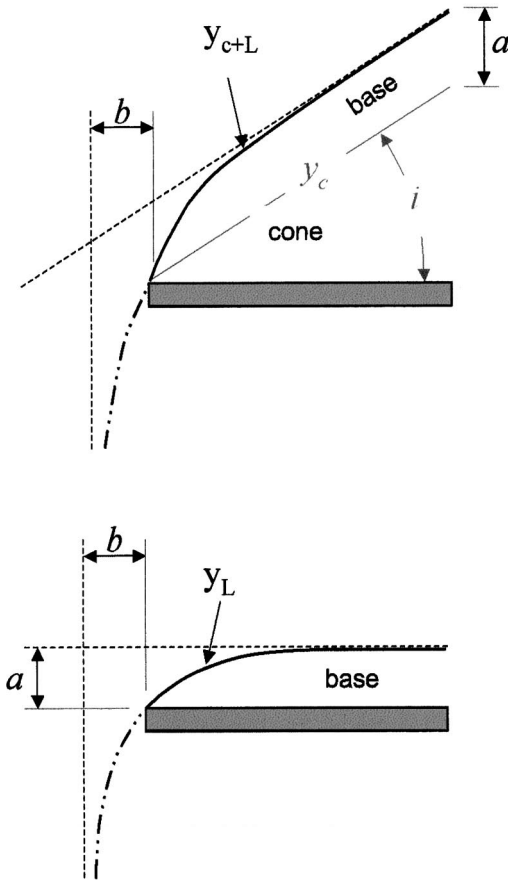


FIG. 5. The upper figure shows the pile at the toe of slope. For the lower figure the cone has been removed.

This upper curve is a distance δ_1 below the asymptote at the corner of the plate ($x = r_m$). From Eq. (13), this displacement is equal to

$$\delta_1 = r_m \tan i - \sqrt{c^2 + r_m^2 \tan^2 i}. \quad (14)$$

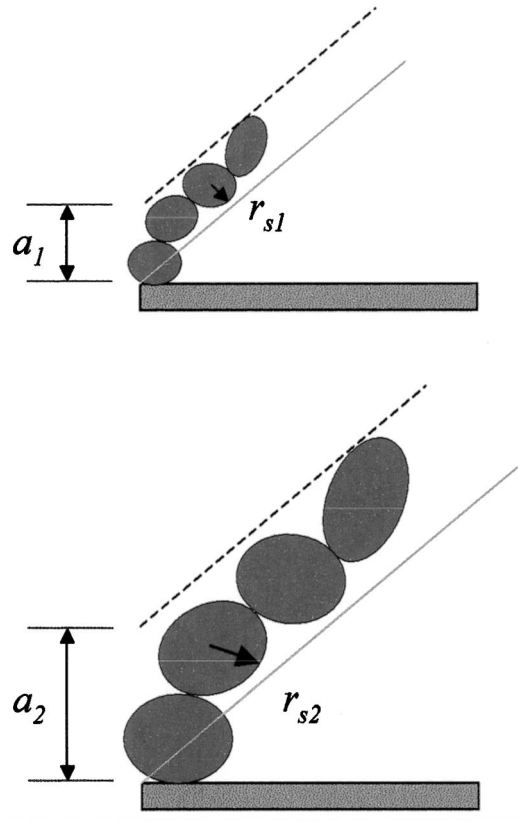
The result is negative indicating that the displacement falls below the asymptote as shown in Fig. 7. For a large pile $\delta_1 \sim 0$. Again c must be normalized to apply to piles with other size sand grains,

$$\bar{c} = \frac{c}{r_s}. \quad (15)$$

The equation for the height of the base is given by the superposition of the curves for the toe of slope and the peak. Hence, summing Eqs. (10), (13), and (14), gives the equation of the base

$$y_b = \frac{a(r_m - |x|)}{b + (r_m - |x|)} + (|x| - r_m) \tan i_m - \sqrt{c^2 + x^2 \tan^2 i_m} + \sqrt{c^2 + r_m^2 \tan^2 i_m}, \quad (16)$$

which for a large pile has a horizontal asymptote at $\approx a$.



$$\frac{a_1}{r_{s1}} = \frac{a_2}{r_{s2}}$$

FIG. 6. a is the asymptote to which the base height approaches. a increases with the size of the sand grains r_s .

Finally, the equation for the height of the base [Eq. (16)] can be combined with the equation for the height of the cone [Eq. (6)] to give the equation for the complete pile as

$$y_p = y_c + y_b, \quad (17)$$

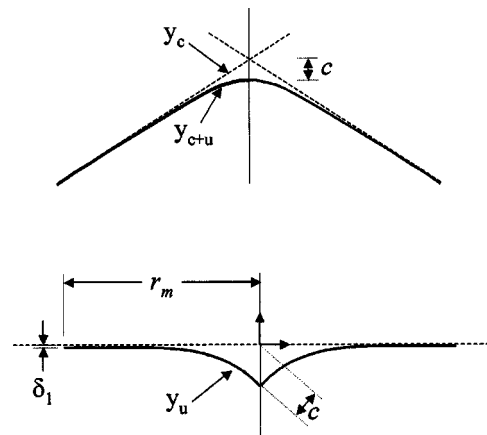


FIG. 7. The upper figure shows the peak of the sand pile. For the lower figure the cone has been removed. Notice that at r_m the value of the curve is not zero, but rather falls a distance δ_1 below the asymptote.

which upon substitution of Eqs. (6) and (16) becomes

$$y_p = \frac{a(r_m - |x|)}{b + (r_m - |x|)} - \sqrt{c^2 + x^2 \tan^2 i} + \sqrt{c^2 + r_m^2 \tan^2 i}. \quad (18)$$

When $a = b = c = 0$, Eq. (18) reduces to the standard cone model in Eq. (6). The volume of the pile is found as the volume of a solid of revolution

$$V_p = 2\pi \int_0^{r_m} x y_p dx, \quad (19)$$

which gives

$$V_p = 2\pi \left[\frac{-(c^2 + r_m^2 \tan^2 i)^{3/2}}{3 \tan^2 i} + \frac{1}{2} r_m^2 (c^2 + r_m^2 \tan^2 i)^{1/2} + a b r_m + \frac{1}{2} a r_m^2 + a b (r_m + b) \ln \left(\frac{b}{b + r_m} \right) \right]. \quad (20)$$

When $a = b = c = 0$, Eq. (20) reduces to the standard cone model in Eq. (8). This equation as written is scalable in r_m for a constant r_s . For application to piles with different but still uniform sand grain sizes, it is necessary to substitute Eqs. (1), (3), (11), (12), and (15), resulting in the specific depth of the pile on a plate D_p ,

$$D_p = \frac{2}{S^3} \left[\frac{-(\bar{c}^2 + S^2 \tan^2 i)^{3/2}}{3 \tan^2 i} + \frac{1}{2} S^2 (\bar{c}^2 + S^2 \tan^2 i)^{1/2} + \bar{a} b S + \frac{1}{2} \bar{a} S^2 + \bar{a} b (S + \bar{b}) \ln \left(\frac{\bar{b}}{\bar{b} + S} \right) \right]. \quad (21)$$

When $a = b = c = 0$, Eq. (21) reduces to the standard cone model in Eq. (9). It is interesting and should be intuitively obvious that as S approaches infinity for larger and larger piles Eq. (21) also approaches the standard cone model in Eq. (9). This model, therefore, predicts that large sand piles are accurately modeled by a standard cone. It can be seen that the initial term with S^3 in the denominator will drive D_p towards infinity for the limiting case where S approaches zero for smaller and smaller piles.

B. Specific depth D_s on a sphere

When making the transformation from Eq. (9) for a standard cone on a flat plate to Eq. (21), two curves were added to account for the curvature at the toe of slope and at the peak. Consider now these curves when the platform is a sphere instead of a flat plate. For the toe of slope, it was shown that the stability provided by a flat plate provided a local increase in i . This dissipated over a few grain lengths distance as shown in Fig. 6, but was the essential factor in producing the curve, which raised the base and increased the volume of the pile. Consider the stacking of sand grains on the surface of a single sphere as shown in Fig. 8. At the toe of slope, the surface of the sphere is inclined at an angle approximately equal to i . Thus, the stability of a sand grain is

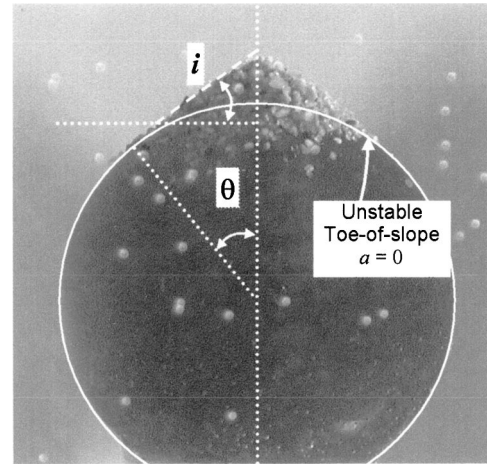


FIG. 8. i and θ for sand grains on the surface of a sphere.

not greater than on the bulk slope; there is no increase in D with r_s as was calculated for the flat platform. For the upper curve at the peak of the pile, the spherical platform pushes the base of the pile higher near the center minimizing the upper curve. The following equations can therefore neglect the curvature of the pile and compare directly with Eq. (9).

The volume of sand on the sphere is an inverted cone with slope i whose base is hollowed by the crown of the sphere. The height of the pile (with respect to the surface of the sphere) at any point is given by

$$y_s = (r_m \sin \theta - |x|) \tan i + r_m \cos \theta - \sqrt{r_m^2 + x^2}, \quad (22)$$

where θ is the angle of friction between the sand grains and the surface of the spherical platform. As a volume of solid of revolution, this becomes

$$V_s = 2\pi \int_0^{r_m \sin \theta} x y_s dx, \quad (23)$$

which solves to

$$V_s = \frac{1}{3} \pi r_m^3 (\sin^3 \theta \tan i - 2 + 3 \cos \theta - \cos^3 \theta). \quad (24)$$

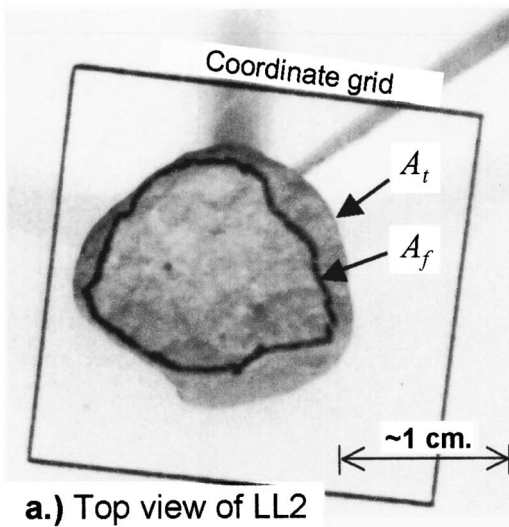
Using Eq. (3) this converts to a specific depth D_s ,

$$D_s = \frac{1}{3} (\sin^3 \theta \tan i - 2 + 3 \cos \theta - \cos^3 \theta). \quad (25)$$

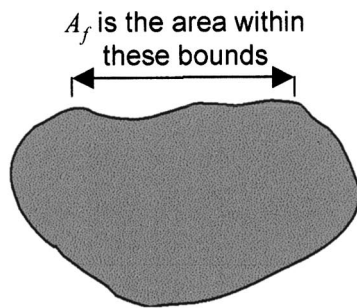
Under the reasonable assumption that the friction between the sand grains and the friction between the grains and the surface for natural materials are approximately equal, i can be substituted for θ in Eq. (25) resulting in

$$D_s = \frac{(1 - \cos i)^2}{3 \cos i}. \quad (26)$$

Thus, the specific depth on a sphere depends only on internal friction of the sand without size effect. For the reasons given above, the contribution of the spherical portion of an irregular platform is not affected by curvature at the toe of slope or the peak. Thus, it can be used without modification in both the cone model and the small pile model discussed below.



a.) Top view of LL2



b.) Schematic Side View

FIG. 9. Both the small pile model and the cone model can be used to approximate an arbitrary shape with a level portion and a spherical portion. The solid black outline on the surface of the limestone shows the boundary of the level surface which defines A_f .

C. Specific depth on an irregular platform

Consider now the irregular surface of a piece of limestone, oriented such that a single facet is level as shown in Fig. 9. The limestone platform has a flat level surface and an outer curved edge. The proportion f of the surface area which is nearly level is given as

$$f = A_f / A_t, \quad (27)$$

where A_f is the total area which is level. $(1-f)$ is the portion of A_t at the curved edges of the platform. The specific depth on the irregular platform, D_{SPM} , can be shown to approximate the weighted linear combination of D_p and D_s , thus, giving

$$D_{SPM} = fD_p + (1-f)D_s \quad (28)$$

or

$$D_{SPM} = \frac{2f}{S^3} \left[\frac{-(\bar{c}^2 + S^2 \tan^2 i)^{3/2}}{3 \tan^2 i} + \frac{1}{2} S^2 (\bar{c}^2 + S^2 \tan^2 i)^{1/2} + abS + \frac{1}{2} \bar{a} S^2 + ab(S + \bar{b}) \ln \left(\frac{\bar{b}}{\bar{b} + S} \right) \right] + (1-f) \frac{(1 - \cos i)^2}{3 \cos i}. \quad (29)$$

Equation (29) is the key result from this paper and will be referred to as the small pile model throughout the remainder of the paper. It is surprising that such a simple model for the shape of a pile (a cone with hyperbolic curves at the toe of slope and peak) results in quite a complicated equation. The values necessary to obtain D_{SPM} for flat plates, spheres, or irregular platforms are \bar{a} , \bar{b} , \bar{c} , i , f , and S , which are all dimensionless.

The small pile model will be compared against the cone model. The cone model results from the linear weighted combination of D_s with D_c .

$$D_{CM} = fD_c + (1-f)D_s, \quad (30)$$

which upon substitution of Eqs. (9) and (26) results in

$$D_{CM} = \frac{f}{3} \tan i + (1-f) \frac{(1 - \cos i)^2}{3 \cos i}. \quad (31)$$

Equation (5) gives a value of the specific depth D from the mass m of the sand pile. Equation (31) is the cone model.

V. METHODS AND RESULTS

A series of experiments was designed and executed to compare the small pile model given in Eq. (29) with the cone model given in Eq. (31). The parameters measured are listed in Table II.

Experiment 1: Determination of r_s , r_m , and S . r_s is the mean sieve size for each sand size fraction given in Table III. To obtain separate sand size fractions, clean dried sand was cross sieved to collect nonoverlapping distributions. Cross sieving differs from ASTM C136 in that sand grains close to the size of the sieve openings are discarded. This was accomplished by sieving the sand twice. The second time using only every other size fraction. The sand was sieved in 200 g samples with 15 min of shaking. Alternate size fractions were set aside and the remainder reintroduced to the top of the sieves for the second sieving and shaken for 3 min, discarding what was not retained on the same sieve. The roundness of the grains of each size fraction was visually inspected (a hand lens was used for the smaller sizes) to confirm that no size fraction was comprised of jagged pieces resulting from the crushing of larger grains. The natural sands used included a range of generally rounded shapes. For piles made up of large numbers of grains, any variability in the shape of individual grains is averaged over the pile, but for piles of only a few grains, the more irregular sand grains are less apt

TABLE II. Parameters needed to compare the small pile model (SPM) and the cone model (CM).

Symbol	Description	Units	Typical Range	Expt. No.	Applies to SPM or CM	From sand size 50 on DSK	
						SPM	CM
Media							
r_m	Radius of presenting area	L		1	Both	38.4 mm	Same
f	Percentage level		Sphere=0 Flat plate=1 Irregular 0-1	2	Both	1.0	Same
A_f	Area which is level	L^2		2	Both	46.33 cm ²	Same
A_m	Total presenting cross-sectional area	L^2		2	Both	46.33 cm ²	Same
Sand							
r_s	Average sand radius	L	See Table III	1	Both	0.181 mm	Same
ρ	Bulk density of sand	M/L^3	See Table III	3	Both	2.69 g/cm ³	Same
Piles							
i	Angle of movement		Glass Beads 20°-25° Sands 30°-40°	4	Both (but different values)	36.7	37.9
ε	Pile porosity		Spheres 25%-47% Nonspherical varies	4	Both	0.510	Same
m	Mass of the pile	M		4	Both	67.0528 g	Same
V	Volume of the pile	L^3		4	Both	509 cm ³	Same
S	Specific size		Small pile < 60	1	Both	212	Same
\bar{a}	Asymptote at toe of slope			4	SPM	9.7	NA
\bar{b}	Asymptote at toe of slope			4	SPM	2.1	NA
\bar{c}	Peak height reduction			4	SPM	20.0	NA

to roll from the pile and are more likely to be retained on the pile.

For spheres or flat plates, r_m was measured with a vernier caliper. For irregular platforms, r_m was calculated using Eq. (2) from the measurements of A_m (see Experiment 2). S was calculated from Eq. (1) for each sand pile.

Experiment 2: Determination of A_m , A_f , and f . The flat surface was outlined on the top of the media grain platform.

TABLE III. Parameters of the sand grain size fractions.

Retained on sieve size	r_s (mm)	ρ (g/cm ³)
6	2.03	2.702
8	1.43	2.683
10	1.09	2.682
16	0.79	2.679
20	0.51	2.684
30	0.37	2.690
40	0.26	2.692
50	0.18	2.686
Mean		2.69
Variance		7.8×10^{-5}

From digitized photographs of these platforms A_m and A_f were measured, then f was calculated using Eq. (27). The photograph of LL2 with coordinate grid is shown in Fig. 9. The results are given in Table IV.

Experiment 3: Determination of ρ . ρ was measured in a liquid pycnometer according to ASTM D854.

Experiment 4: Determination of \bar{a} , \bar{b} , \bar{c} , i , ε , m , and V . The pile parameters were measured from a large pile to prevent interference of the curve at the toe of slope at the peak and vice versa. The small pile model and the cone model were tested for small piles in Experiment 5 using the parameters measured from this large pile. Figure 1(f) shows the sand grains delivered with a small spatula directly to the surface of the pile, perpendicular to the direction of motion. For sand with r_s greater than 0.75 mm the grains were generally deposited one by one at the point of greatest apparent stability. For r_s below 0.75 mm the grains were deposited in small groups, the number of grains increases to about 5-10 for r_s down to 0.15 mm. Use of the spatula minimized the impact velocity over the entire range of S .

Because the intended application of the work was the storage of noncolloids in a filter, the sand grains piles were formed underwater. Adding the sand grains underwater further reduced the velocity of the impacting sand grains and

TABLE IV. Parameters of the platforms.

Platform	Description	r_m (cm)	A_m (cm ²)	f
Experiment 4				
DSK-L	Large smooth flat metal disk	3.84	46.33	1
Experiment 5				
SP	Deglossed glass marble	0.79	1.93	0
LL1	Limestone piece	0.75	1.74	0.30
LL2	Limestone piece	0.83	2.16	0.67
LL3	Limestone piece	0.72	1.61	0.06
DSK-R	Rough flat metal disk	0.90	2.51	1

eliminated any effects from humidity. It has been shown that underwater i exhibits an increase with absolute grain size [13]. Using this reported increase, Table V shows the values of i used in the second experiment to test the small pile model. Grains were added until approaching i , when the experiment was stopped (generally after i had been exceeded several times with resulting avalanches.) The sand pile was then photographed, collected from the underwater, and subsequently dried and weighed.

Five samples were collected from a flat disk (DSK-L) using sand size 50. Photographs were taken for each pile. One is shown in Fig. 3. The grid in the background of each picture was not used directly to measure the outline of the pile (because of parallax), but simply to correct for spherical aberration of the photograph image. Aberration was consistently less than 1 percent in any direction. The photographs were scanned and the outlines digitized in AUTOCAD®. Control points for scale were the edges of the platform. The points were then exported to MATLAB® for detailed analysis. From the five outlines, an average pile shape was determined. Figure 10 shows the average outline of sand size 50 ($r_s = 0.18$ mm) on DSK-L ($r_m = 38.4$ mm). The values of i , \bar{a} , \bar{b} , and \bar{c} taken from this average outline are provided in Table II. Figure 10 shows the plot of Eq. (18) on this outline using the values of Table II. Measurement error of i was less

TABLE V. Values of i for test of the models using mean i from Experiment 4 (Table II) and correction by Courrech du Pont *et al.* [13].

Sand size	i_{measured} (deg)	Correction	i (deg)
50	36.70	0	36.70
40		0.33	37.03
30		0.66	37.36
20		0.97	37.67
16		1.40	38.10
10		1.70	38.40
8		1.95	38.65
6		2.28	38.98

than 1°, but it was taken from a two-dimensional picture and assumed to apply around the entire surface of the three-dimensional pile; thus, it may contribute to the variance in values of D .

The pile volume V was calculated from the photographs (see Fig. 3) by integrating a solid of revolution. The pile mass m was measured from the collected dried sand. The pile porosity ε is given by

$$\varepsilon = 1 - \frac{m}{V\rho}. \tag{32}$$

This completes the measurement of all of the parameters needed to compare the performance of the sand pile models.

Experiment 5: Small piles on natural surfaces; testing the models. Having measured all of the parameters necessary, the small pile model was tested against the cone model on the natural surfaces of various media [a sphere (SP), limestone fragments (LL1, LL2, LL3), and a flat disk (DSK-R)]. These platforms are shown in Fig. 11. Sand piles were pre-

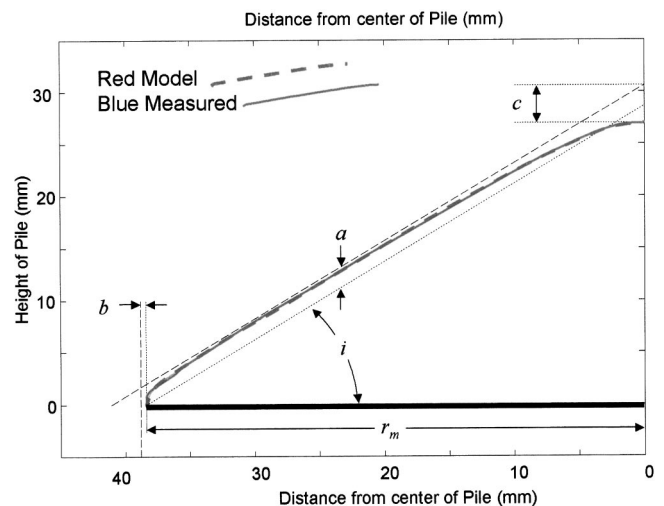


FIG. 10. Measurement of a , b , c , and i from sand size 50 on DSK-L in Experiment 4. Note that the dimensions shown labeled as a and c are only such for a large pile.

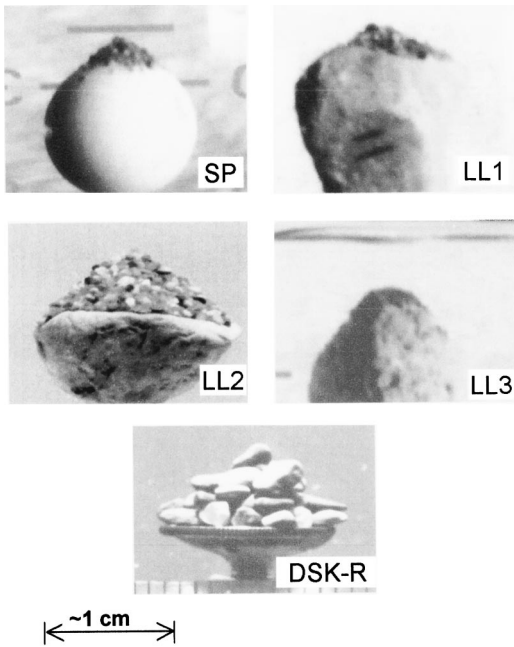


FIG. 11. Irregular platforms used in Experiment 5.

pared as described in Experiment 4. The sphere was a glass marble with the glossy coating stripped off in a rock tumbler with fine abrasive. Eight sizes of sand were used (50, 40, 30, 20, 16, 10, 8, and 6). Each sand size is shown on platform LL2 in Fig. 12. The experiment was repeated five times for each sand size on each platform.

VI. DISCUSSION AND CONCLUSIONS

Figure 13 shows D vs S for each sand grain size fraction on each natural surface. The small pile model predictions

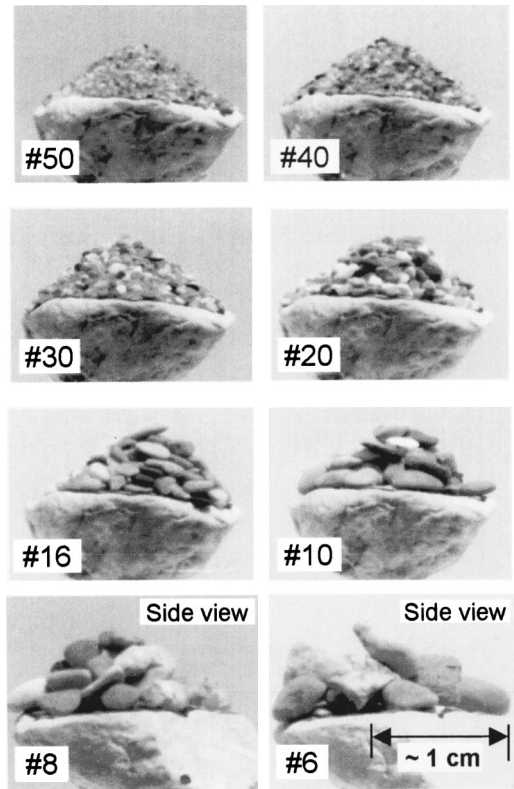


FIG. 12. Various sand sizes on LL2 as used in Experiment 5.

given by Eq. (29) and the cone model predictions given by Eq. (31) are also plotted in Fig. 13. Tabular values are provided in Table VI. The cone model predicts straight lines with nearly zero slope (the slight slope results because the piles are formed underwater [13]). As previously mentioned, the predictions of the small pile model converge with the

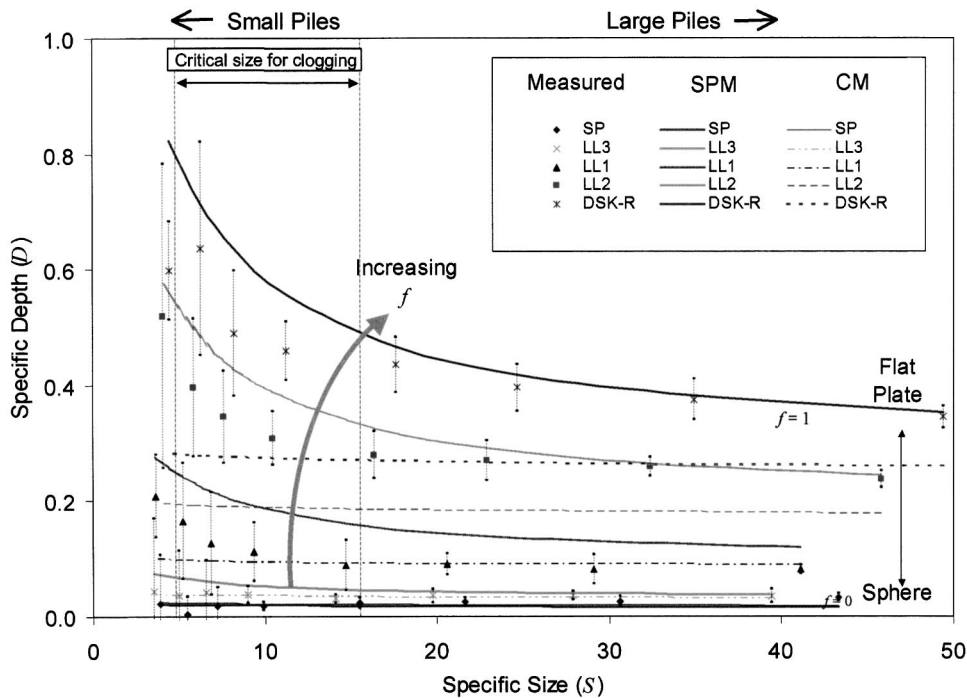


FIG. 13. Specific depth of sand piles on the various irregular platforms in Experiment 5. Solid lines are the small pile model predictions and dashed lines the cone model predictions. Error bars are three standard deviations.

TABLE VI. Results from Experiment 5 shown in Fig. 13.

<i>S</i>	<i>D</i>		Small pile model		Cone model	
	Mean	Variance	Value	Relative error	Value	Relative error
SP (<i>f</i> =0)						
43.3	0.033	4.2×10^{-6}	0.016	-0.50	0.019	-0.43
30.6	0.026	7.6×10^{-6}	0.017	-0.35	0.020	-0.25
21.7	0.025	6.1×10^{-6}	0.018	-0.30	0.020	-0.19
15.5	0.023	1.0×10^{-5}	0.018	-0.21	0.021	-0.09
9.9	0.018	6.0×10^{-6}	0.019	0.04	0.022	0.20
7.2	0.018	1.2×10^{-4}	0.020	0.11	0.023	0.28
5.5	0.004	9.7×10^{-5}	0.020	3.59	0.024	4.27
3.9	0.021	8.1×10^{-4}	0.021	0.01	0.024	0.16
LL1 (<i>f</i> =0.30)						
41.10	0.080	5.6×10^{-6}	0.120	0.46	0.090	0.10
29.07	0.080	7.2×10^{-5}	0.130	0.58	0.092	0.12
20.55	0.088	3.7×10^{-5}	0.143	0.58	0.093	0.03
14.68	0.087	2.1×10^{-4}	0.160	0.81	0.095	0.07
9.37	0.110	2.9×10^{-4}	0.191	0.70	0.096	-0.14
6.83	0.125	8.7×10^{-4}	0.218	0.70	0.098	-0.23
5.21	0.163	1.1×10^{-3}	0.243	0.46	0.099	-0.40
3.67	0.205	5.7×10^{-4}	0.276	0.32	0.101	-0.52
LL2 (<i>f</i> =0.67)						
45.79	0.235	2.3×10^{-5}	0.244	0.02	0.180	-0.25
32.39	0.256	3.1×10^{-5}	0.264	0.02	0.182	-0.30
22.90	0.267	1.3×10^{-4}	0.291	0.07	0.185	-0.32
16.35	0.276	1.9×10^{-4}	0.326	0.16	0.187	-0.34
10.44	0.305	2.3×10^{-4}	0.390	0.26	0.190	-0.39
7.61	0.342	7.0×10^{-4}	0.446	0.28	0.192	-0.45
5.80	0.379	1.6×10^{-3}	0.499	0.25	0.194	-0.51
4.09	0.514	7.7×10^{-3}	0.573	0.10	0.196	-0.62
LL3 (<i>f</i> =0.06)						
39.45	0.035	1.5×10^{-5}	0.037	0.06	0.033	-0.06
27.90	0.035	5.8×10^{-6}	0.040	0.12	0.034	-0.05
19.72	0.035	1.5×10^{-5}	0.043	0.22	0.035	-0.02
14.09	0.031	6.4×10^{-6}	0.048	0.53	0.036	0.15
8.99	0.038	2.4×10^{-5}	0.055	0.42	0.037	-0.03
6.56	0.041	3.5×10^{-4}	0.061	0.46	0.038	-0.08
5.00	0.037	6.6×10^{-4}	0.066	0.78	0.039	0.04
3.53	0.043	1.8×10^{-3}	0.074	0.68	0.040	-0.09
DSK-R (<i>f</i> =1)						
49.38	0.342	3.9×10^{-5}	0.353	0.02	0.260	-0.25
34.93	0.371	1.4×10^{-4}	0.381	0.01	0.263	-0.30
24.69	0.392	1.8×10^{-4}	0.418	0.05	0.266	-0.33
17.64	0.431	2.6×10^{-4}	0.466	0.07	0.269	-0.39
11.26	0.455	2.8×10^{-4}	0.556	0.20	0.273	-0.41
8.21	0.486	1.3×10^{-3}	0.636	0.29	0.276	-0.44
6.26	0.630	3.8×10^{-3}	0.715	0.12	0.279	-0.56
4.41	0.593	8.1×10^{-4}	0.824	0.37	0.282	-0.53

predictions of the cone model when the piles are large (as *S* goes to infinity). In general, the predictions of the small pile model are biased above the measured data points. This may result from several causes. In the case of LL1, LL2, and LL3, the delineation of the boundaries of the flat surface result in

some error in the measurements of *f*. However, this should result in a bias at all values of *S*, whereas, the predictions of the small pile model at larger values of *S* are quite good. Another possible reason is that the surfaces of the natural shapes (in Experiment 5) have greater variability than the flat

plate from which the parameters were measured (Experiment 4). However, this bias should extend to the entire range and again the small pile model fits well at higher values of S . Most likely, the deviation as S decreases results from discrete effects of the sand grains as the pile size decreases. (Remember the more angular grains are less apt to roll from the pile.)

The small pile model is based on the difference between a flat platform's inherent stability at the toe of slope, which provides a local increase in the angle of movement (Fig. 6) and the inherent instability at the toe of slope on a sphere (Fig. 8). For a flat platform the increase in the angle of the pile at the toe of slope disappears over some small number of grain contacts resulting in a hyperbolic shape. A similar curve is observed at the peak. Incorporating these curves results in a scalable model (the small pile model) which accurately predicts the volume of sand in both large and small piles. This is a significant improvement over the cone model which accurately predicts the volume of large piles but is not scalable to small piles. The small pile model also agrees with the experimental results which show that spheres do not have an increase in the size of the sand pile as the sand grains increase. At the toe of slope of a sand pile on a sphere, the angle of the surface is approximately inclined at the angle of the sand, thus, the toe of slope has no greater stability to locally increase the angle of the pile.

Two important conclusions are reached about the formation of small sand piles. First, as f increases D increases, thus

in a packed filter bed, crushed material could provide for significantly greater particle removal than for spheres. Second, for crushed shapes the measurements confirm the prediction of the small pile model that D increases significantly as S decreases in the critical size range for clogging. This increase has implications for the clogging of filter media, and is properly predicted by the small pile model, but not the cone model. In filtration as the incoming particle size increases so does the mass of particles stored on the leading edge of the filter grains even before clogging occurs. An increase in the pile size will allow for greater internal clogging of filter media.

This analysis is based on uniform particle sizes and has not yet been compared with results from a graded sample. The improved mass stored on the irregular surfaces strongly suggests that for any distribution of sizes small enough to enter the media, the mass removal will be greater for crushed media than for spherical.

Major points are the following:

(1) The small pile model derived from hyperbolic curves at the toe of slope and the peak provides a reasonable prediction of the mass stored in irregular grains.

(2) Flat plates and irregular surfaces have greater mass of sand piles with larger sand grains.

(3) Spheres have no change in mass stored with sand size because the toe of slope is not stable.

-
- [1] V. B. Pandya, S. Bhuniya, and K. C. Khilar, *AIChE J.* **44**, 978 (1998).
- [2] R. Sakthivadivel, Hydraulic Engineering Laboratory Report No. HEL 15-5, 1966 (unpublished).
- [3] R. Sakthivadivel, Hydraulic Engineering Laboratory Report No. HEL 15-7, 1969 (unpublished).
- [4] J. Duran, *Sands, Powders, and Grains: An Introduction to the Physics of Granular Materials* (Springer-Verlag, New York, 2000).
- [5] C. H. Lui, H. M. Jaeger, and S. R. Nagel, *Phys. Rev. A* **43**, 7091 (1991).
- [6] W. A. Gray, *The Packing of Solid Particles* (Chapman and Hall, London, 1968), pp. 28, 50.
- [7] A. Van Burkalow, *Bull. Geol. Soc. Am.* **56**, 669 (1945).
- [8] F. Auerbach, *Ann. Phys.* **4**, 170 (1901).
- [9] M. Carrigy, *Sedimentology* **14**, 147 (1970).
- [10] Y. C. Zhou, B. H. Xu, A. B. Yu, and P. Zulli, *Powder Technol.* **125**, 45 (2002).
- [11] J. T. Carstensen and P.-C. Chan, *Powder Technol.* **15**, 129 (1976).
- [12] H. M. Jaeger, C. Lui, and S. Nagel, *Phys. Rev. Lett.* **62**, 40 (1989).
- [13] S. Courrech du Pont, P. Gongret, B. Perrin, and M. Rabaud, e-print cond-mat/0209059.
- [14] G. A. Held *et al.*, *Phys. Rev. Lett.* **65**, 1120 (1990).
- [15] S. K. Grumbacher, K. M. McEwen, D. A. Halverson, and D. T. Jacobs, *Am. J. Phys.* **61**, 329 (1993).